**Classification**
PHYSICAL SCIENCES: Biophysics and Computational Biology
BIOLOGICAL SCIENCES: Microbiology

**Title**

# Swarming bacteria undergo localized dynamic phase transition to form stress-induced biofilms

**Authors**
Iago Grobas[1], Marco Polin[1,2,3,*†] & Munehiro Asally[4,5,6,*†]

**Affiliations**
[1]Warwick Medical School; [2]Centre for Mechanochemical Cell Biology; [3]Physics Department; [4]Bio-Electrical Engineering Innovation Hub; [5]Warwick Integrative Synthetic Biology Centre; [6]School of Life Sciences, University of Warwick, Coventry, CV4 7AL, UK
†Equal contribution

*Corresponding Authors
Marco Polin: m.polin@warwick.ac.uk
Munehiro Asally: m.asally@warwick.ac.uk

**Abstract**
Swarming and biofilm formation are two modes of bacterial collective behavior that enable cells to increase their tolerance to anti-microbial stressors. Swarming is a rapid type of surface colonization, and therefore its ability to withstand high antibiotic concentrations could lead to the subsequent establishment of highly resilient biofilms in regions that could not otherwise have been colonized. However, whether swarms can transit into biofilm at all, and how, remains unclear. Using *Bacillus subtilis*, we reveal that a biophysical mechanism, reminiscent of motility-induced phase separation (MIPS), underpins a swarming-to-biofilm transition through a localized dynamic phase transition. Guided by the MIPS paradigm, we demonstrate that the transition is triggered by environmental stressors such as an antibiotic gradient or even a simple physical barrier. Based on the biophysical insight, we propose a promising strategy of antibiotic treatment to effectively inhibit the transition from swarms to biofilms, by targeting the localized phase transition. The biophysical origin of such a transition suggests that biophysics-based approaches could emerge as a potential tool to control and understand collective stress response in bacterial communities.

**Keywords**
Cell biophysics; Quantitative Biology; Swarming; Biofilms; Motility-induced phase separation; Active Matter

**Significance Statement**
Bacteria can organize in different types of communities to better tolerate stresses taking advantage of novel properties that lack in the planktonic state. Here we show that bacterial swarms, characterized by a rapid group motility on a surface, can use a biophysical mechanism resembling motility induced phase separation to transit into biofilms, a more resistant form of bacterial collectives. The transition is promoted by a slowing down in the swarm expansion, leading to the subsequent accumulation of multiple layers of bacteria near the swarming front. Such accumulation results in large inhomogeneities in cell density which triggers wrinkle formation, the morphological feature of biofilms. Our data suggest that wrinkle formation can be inhibited can be inhibited by locally targeting the swarming front, where the phase transition takes place.

## MAIN TEXT

### Introduction

The ability to sense, respond and adapt to varieties of environmental conditions and stresses is crucial for the survival of species (1–3). Biofilm, structured communities of microbes embedded in extracellular polysubstance (EPS), has been considered as a type of stress response due to its elevated tolerance against various stresses, including antibiotics, extreme pH and temperature (4–7). The biofilms' resilience is associated with physicochemical properties of EPS (8), metabolic coordination (9), slow cell growth (10), and in the case of air-exposed biofilms, diffusion barrier by archetypical wrinkled morphology (11, 12). Biofilm formation can be induced, from planktonic cells, by a wide range of biochemical and mechanical stressors, such as aminoglycoside antibiotics (13), redox-active compounds (14), nutrient depletion (15) and mechanical stress (16). Swarms, another form of bacterial collectives, can also collectively tolerate antibiotic treatments that are lethal to individual cells -albeit to a lesser degree than biofilms- through motility-induced mixing and reduced small-molecule uptake (17–20). However, whether swarming collectives may transit into more resilient biofilms when exposed to stressors, and if so, how collective transition can be initiated, is unknown.

Understanding biophysical mechanisms regulating the emergence of tolerance through bacterial collective behavior is emerging as an important research focus (21–23). For example, collectively moving clusters of planktonic *E. coli* cells can colonize regions of high antibiotic concentration only when the cluster is above a threshold size (24), highlighting the potential biological advantages of structures that can emerge spontaneously in a group, as a consequence of the physics of cell motility. Research on the biophysics of collective motion in bacteria has a long history, dating back to the seminal work of Vicsek on flocking (25), and it is now a major topic within the rapidly growing area of active matter (26, 27). Theoretical models of active matter have repeatedly predicted that, at a sufficient concentration, a collection of motile particles can spontaneously form high-density clusters of particles (28, 29). Indeed, this process has been already implicated in the development of cell inhomogeneities leading to fruiting-body formation in gliding *M. xanthus* (30). This transition, known as Motility Induced Phase Separation (MIPS), is based on feedback between the decrease in particles' speed at high concentration, caused by physical interactions, and the spontaneous accumulation of active particles in the places where their speed is lower (28). When the particles' speed is sufficiently high and their concentration is in the appropriate range (typical volume fractions of 0.3-0.8 or 0.6-0.7 for round or rod-shaped particles, respectively (31, 32)), inherent density fluctuations are amplified by the particles' slowing down, and the system effectively phase separates into high-density/low-motility clusters surrounded by a low-density high-motility phase (33).

The theory of MIPS, then, suggests that persistent heterogeneity in cell density -the MIPS clusters- can develop spontaneously when both cell speed and density are appropriate (Fig.1, grey U-shape region) (34) Such conditions should be achievable within a bacterial swarm. Given that cell-density heterogeneity can induce biofilm formation mediated by localized cell death (35, 36), we wondered whether the heterogeneity caused by putative MIPS-like clusters could in turn underpin the transition from bacterial swarms into biofilms (Fig. 1). As MIPS-like clustering is an emergent phenomenon arising from physical interactions between individual agents, it may endow swarms with a collective response to a wide spectrum of stressors that cause changes in cell motility and/or density.

Here we show that *Bacillus subtilis* swarms can indeed transit into biofilms through a MIPS-like process, induced by physical or chemical stresses applied at the swarming front. The stresses promote a localized phase transition where the expanding swarm monolayer generates multilayer clusters of cells. Based on the insights gained from our investigation, we then show that targeting the multi-layered region by administering a given amount of antibiotic in two separate doses is effective in suppressing the formation of biofilms from swarming cells.

### Results

#### Swarming *B. subtilis* transits into a biofilm in presence of a spatial kanamycin gradient

To examine if a stressor may trigger biofilm formation from a swarming collective, we performed swarming assays using *B. subtilis* with a spatial gradient of the aminoglycoside kanamycin. Specifically, a disk containing 30 μg of kanamycin was placed on the side of a swarming plate (0.5% agar) and allowed to rest for 24 hours to establish a space-dependent antibiotic concentration profile (Fig. 2a and S1). An inoculum of *B. subtilis* culture was then placed at the center of the dish, ~4 cm away from the kanamycin source, and the plate was imaged while being kept at 30°C (Fig. 2a). After ~2 hours of lag period, the cells formed a rapidly expanding swarming front (~4 mm/h), which became progressively slower towards the source of kanamycin until it completely stopped ~0.3 cm away from the disk (Fig. S2 and Supplementary Video 1). After further incubation at 30°C for 36 hours, the colony developed prominent wrinkles, the morphological hallmark of pellicles and colony biofilms (12, 37), across a ~3 mm band ~1.3 cm away from the kanamycin disk (Fig. 2b). The estimated level of kanamycin at the site was nearly half the minimum inhibitory concentration (MIC) (Fig. S1). To quantify the degree of biofilm formation, we measured the characteristic wavelength and roughness of the wrinkles, which have been reported to correlate with biofilm stiffness (35, 38, 39). The wrinkles appearing near the kanamycin disk had a wavelength of $\lambda = 560$ μm and roughness $r = 10$, while those without kanamycin only produced a faint small-wavelength surface roughness ($\lambda = 91$ μm, $r = 5.5$; Fig. S3).

To verify the association of these wrinkles to biofilms, we repeated the assay using *Δeps*, a mutant known to be impaired in biofilm formation (40) but capable of swarming (Supplementary Video 2), and confirmed no wrinkles with this mutant (Fig. 2c). Furthermore, a strain carrying $P_{tapA}$-*yfp,* a fluorescence reporter for the expression of *tapA-sipW-tasA* operon (41), showed an upregulation of the promoter activity when swarming cells are exposed to kanamycin (Fig. 2e), indicating the stress-induced activation of biofilm formation on a swarming agar plate.

The emergence of wrinkles signals that the system transits from a swarm to a biofilm in correspondence to exposure to a certain concentration range of kanamycin. Indeed, increasing the initial concentration of antibiotic in the disk, wrinkles emerged further away from it (Fig. S4), while a disk without antibiotic did not promote wrinkle formation (Fig. 2d). Intriguingly, on hard agar plates (1.5%), wrinkles were only induced to a lesser extent than in the swarming case (Fig. S5). The fact that a kanamycin gradient promotes wrinkle formation in a swarming colony, but not in a non-motile culture, pointed to a fundamental role played by cell motility and suggested the need to investigate the swarming dynamics in detail.

**The emergence of the biofilm is templated by a transition from mono- to multi-layers localized at swarming front**

To investigate the potential link between swarming dynamics and biofilm formation, we characterized the swarming dynamics at the single-cell level, with and without a kanamycin gradient. We combined time-lapse imaging at both microscopic (10×; 30 fps) and macroscopic (2×; 0.006 fps) scales to capture both swarming, which is microscopic and fast (~70 $\mu m^2$ cell rafts; speed ~60 μm/s), and biofilm formation, which occurs at a macroscopic scale over hours to days. For the microscopic imaging, we focused on the cells at ~1 cm from the kanamycin disk, where wrinkles eventually appear and kanamycin level is below MIC (Fig. S1). The cells displayed typical swarming dynamics during the expansion of the colony front (Fig. 3a). As time progressed we observed the local surface coverage of the monolayer swarm to progressively increase from initial values of ~20% to ≳60%, at which point the swarming rafts started displaying jamming events lasting ~1-2 sec, during which groups of cells protruded temporarily from the swarming monolayer (typical size of jammed group ~500 $\mu m^2$, see Supplementary Video 3 and Figs. 3a,b).

The jamming of aligned rafts has been predicted numerically for elongated self-propelled particles on a plane (42, 43) although in that case the planar confinement precluded any possible excursion in the third dimension. With a slight further increase in local cell density, the temporary jams led to permanent isolated multi-layered regions, which we call 'islands', typically ~27,000 $\mu m^2$ in size and with constantly fluctuating boundaries (Fig. 3b inset, Supplementary Video 4). The islands did not appear to be related to any evident inhomogeneity of the underlying agar. Within islands, cells were highly dynamic and appeared to meander across the layers albeit at a reduced speed. Cell movement within islands (Fig. S7, Supplementary Video 5) highlights the fact

that these islands are formed by actively motile cells, rather than groups of immotile bacteria which spontaneously separate from the monolayer. In particular, we did not find any evidence for clusters of immotile cells templating the islands. Rather, motile cells were constantly exchanged between the multilayer and the surrounding monolayer. Following a continuous increase in cell density with time, islands grew in size and merged with each other, eventually forming a much larger multi-layered region (Fig. 3c, Fig S7, Supplementary Video 6). The nucleation and merging of islands were observed up to 4 layers before we lost the ability to recognize further transitions due to a flattening of the image contrast (Fig. S7).

The formation of islands was also observed by macroscopic time-lapse imaging. In absence of kanamycin, islands emerged simultaneously throughout the plate, forming an intricate granular pattern with a typical size of ~2,000 $\mu m^2$ (Fig. 3d), a phenomenology reminiscent of spinodal decomposition in binary fluids (44). In contrast, the process of islands formation and growth was markedly different in presence of kanamycin (Fig. 3e). Following the halt of the swarming front expansion due to inhibition by the antibiotic, well-defined, distinct islands emerged well separated and only within a ~5mm-wide band just inside the arrested swarming front, and then grew with a strongly anisotropic pattern oriented transversally to the front of the swarm (Video S6). This phenomenology is reminiscent of a binodal -rather than spinodal- liquid-liquid phase separation in a temperature gradient (45) which here might reflect a kanamycin-induced speed gradient. The latter macroscopic cell-density heterogeneity resulted in the subsequent formation of biofilm wrinkles, ~1 cm away from the disk (Fig. 2b).

Since quorum sensing is often associated with bacterial collective behavior, we wondered if quorum sensing may play a role in the emergence of islands and the ensuing multilayer. We therefore repeated the experiments with *ΔphrC* and *Δopp* mutant strains, lacking the Phr quorum-sensing system in *B. subtilis* but still capable of swarming. In both cases, we observed the wild-type phenomenology of wrinkled biofilms and the emergence of islands (Fig. S8). The results indicated that this quorum-sensing system is not responsible for the multi-layer transition, suggesting that exposure to kanamycin can promote cell-density heterogeneity by multi-layer islands formation in a quorum-sensing independent manner.

**Transition from monolayer to multilayer resembles motility induced phase separation**

To address the mechanism of multi-layer formation, we wondered if physical stresses may be responsible for this emergent collective behavior since single-to-multi layer transitions have been reported for confined bacterial aggregates, either growing or gliding, as a consequence of build-up of internal mechanical stresses (46, 47). In particular, we considered if the active matter model of MIPS for rod-shape particles (33) could act as a useful paradigm for understanding the emergence of multi-layer regions. We therefore mapped our experimental results onto the typical phase space considered when studying MIPS transitions, where an active 2-dimensional system is characterized by its surface coverage, $\varphi$, and its rotational Péclet number, $Pe_r = u/LD_r$. The latter is defined in terms of the average speed u, characteristic size L, and rotational diffusivity $D_r$ of the active particles. MIPS clusters are expected within a U-shaped region characterized by a sufficiently large $Pe_r$ and a range of surface coverages that, for rod-like particles like *B. subtilis*, is pushed to values higher than the ~50%, typical of circular particles, due to antagonistic effects of cell-to-cell alignment (32) (Fig. 4a, grey U-shape region shows the prediction for aspect ratio 2 from [37]). We then quantified the cell density (surface coverage, $\varphi$) and the rotational Péclet number from the different stages of the swarming process. Figure 4a shows these two quantities for cells in the monolayer (blue dots) and for bacterial jams (red dots). While bacteria in the monolayer corresponded overwhelmingly to points well outside the MIPS region (Fig. 4a blue dots), bacterial jams -the first stage in the development of stable multilayer islands- clustered around the area predicted for MIPS in two-dimensional self-propelled rods (Fig. 4a, red dots; MIPS region from [35]). Jamming events were also characterized by a sudden drop in cells' speed (Fig. 4b and Supplementary Video 3), consistent with the basic premise of MIPS. Altogether, these results show that the mechanism leading to the development of multilayered islands is compatible with the MIPS process in active matter. Having established the similarities between MIPS and multilayer formation in the swarm, it is important to test the ability of the model to predict the results of new experiments.

**Local accumulation of swarming cells induces multilayer transition and biofilm formation**

The MIPS paradigm makes the experimentally testable prediction that it should be possible to induce multilayer formation by altering the local density of motile cells, thereby forcing the system to enter the MIPS region in phase space (Fig. 4a, shaded region). We tested this in two ways: by UV irradiation, and through the use of a physical barrier to block front expansion. Near-UV light can decrease cell speed in gram-negative bacteria like *E. coli* and *S. marcescens* (48, 49), as well as, as we report here, in *B. subtilis* (Fig. S9a). Locally slowing down motility by light can lead to a local increase in cell concentration through the accumulation of cells from non-irradiated regions (Fig. 4c). We first verified that the illumination by UV light itself does not induce a multilayer transition, by illuminating an area >200-fold greater than the field of view. This prevented cells outside of the irradiated area from accumulating within the field of view during the experiment. Accordingly, the surface coverage increased only marginally ($\varphi \simeq 0.45$ to $\varphi \simeq 0.47$ in 3 min; Fig. S9a). The UV illumination caused an initial sudden drop in average speed from 65 μm/s to 50 μm/s (Fig, S9a), followed by a nonlinear progressive slow down over the course of 3 min. Within the phase space picture (Fig. 4a, Fig. S9b), this corresponds to a trajectory that essentially just moves towards progressively lower values of $Pe_r$. This should not lead to either jams or island formation, which in fact were never observed (Fig. 4a, Fig. S9b). We next illuminated a region of size similar to the field of view. This arrangement allowed cells from the outer region to accumulate within the field of view due to UV-induced slow-down, a phenomenon which is a direct consequence of the active, out-of-equilibrium nature of the swarm with no counterpart in statistical systems in equilibrium (50–52). As a consequence, the cell density increased significantly ($\varphi \simeq 0.42$ to $\varphi \simeq 0.7$ in 2 min; Fig. 4c). For the first ~2 min, the average drop in cell speed was likely compensated by the density increase. It is well known, in fact, that cell density can enhance swarming motility through cooperative raft formation (53, 54). Eventually, however, the increase in cell density resulted first in the formation of jams and finally of multi-layer islands (Fig. 4c, Supplementary Video 7). Figure 4d shows the trajectories followed by the irradiated swarms in phase space. Jamming of swarming cells, the first step in island formation, occurs only for cell densities within a range that compares very well with predictions by MIPS for self-propelled rod-like particles (Fig. 4d shaded region and (32)). These results provide a direct support to the hypothesis that a biophysical MIPS-like process underpins the transition from swarming monolayers to multilayers in *B. subtilis*.

To further examine if a local cell-density increase is sufficient by itself to induce a localized transition from monolayer to multilayer, we used a physical barrier to impede the advance of the swam and locally increase cell density. Again, consistently with the MIPS picture, the arrest of the swarm front led to an increase in cell density and the subsequent emergence of multi-layer islands near the barrier (Supplementary Video 8). After 36 hours of further incubation, wrinkles developed near the physical barrier precisely in the region where the islands had started to appear initially (Fig. 5a).

Altogether, these results strongly support that *B. subtilis* swarms can undergo a single-to-multi-layer transition driven principally by a physical mechanism compatible with MIPS, which can be either global and spinodal-like, or localized and binodal-like. When this transition is localized, regardless of it being caused by antibiotics or physical confinements, the resultant macroscopic cell-density heterogeneity determines the emergence of wrinkled biofilms.

**Sequential administration of antibiotics suppresses the emergence of biofilms from swarms**

While a range of complex signaling pathways are likely involved in the passage from localized multi-layers to wrinkles, our results suggest that altering the expansion dynamics of a swarm promotes biofilm formation. This implies that exposing bacterial swarms to stressors, such as kanamycin, physical barrier and UV light, may inadvertently increase their resilience by promoting the formation of biofilms that are much more difficult to eradicate. This is difficult to prevent by simply increasing the amount of antibiotics. In fact, when we used a ~7-fold greater dose of kanamycin in the diffusion disk (200 μg), wrinkles still appeared on the plate, although at a greater distance from the disk (Fig. S4). However, our findings suggest that the multi-layer band could be a good target for antibiotic treatment aimed at suppressing the emergence of biofilms. Such multilayer band happens at a concentration of antibiotic that bacteria can tolerate since the cells are still motile (in our case ~0.5 MIC; see Fig. S6, Supplementary Video 5). We therefore wondered if a two-step sequential antibiotic administration could prevent biofilm formation, where the first administration induces multilayer formation and the second targets the multilayer area before completing biofilm formation. To test this conjecture, we

decided to administer a total amount of 200 µg of kanamycin in two steps, an initial one when placing the disk on the plate, and the second as the swarming front stopped (Fig. 5b, Fig. S10). The emergence of wrinkles was greatly suppressed when kanamycin was administrated sequentially, despite keeping the total amount of antibiotic constant (Fig. 5b,c and Fig. S10). The effect was most evident when the second dose was greater than the first. These results thus propose a promising strategy for treating bacterial collectives with aminoglycoside while minimizing the emergence of biofilms.

## Discussion

This work reveals a biophysical mechanism underpinning the emergence of biofilms from swarms in *B. subtilis* through a localized phase transition governed by motility and cell density. We demonstrated that the transition from monolayer to multilayer can be induced by qualitatively different means, from antibiotics to UV and physical confinement. Based on our findings, we showed that a sequential monotherapy can be effective in preventing biofilm formation from a swarming colony in *B. subtilis*. As the underpinning mechanism of the transition is an emergent phenomenon driven by physical interactions between swarming cells, we believe similar transitions could happen in other bacterial species. It would be interesting, for example, to examine if swarms of clinically relevant bacteria, such as *Pseudomonas aeruginosa* and *Salmonella enterica,* may also transit into biofilms through a similar process. Such investigations would be an important step to see if sequential administrations could be effective in preventing stress-induced biofilm formation also in pathogenic bacteria.

This study addresses a fundamental question about the mechanism by which cell collectives adapt their behavior in response to various physical and chemical environmental cues. Our findings suggest that a local cell-density increase may be a general environmental sensing mechanism that allows swarming bacteria to transit into biofilms. Such a sensing mechanism could allow the swarming collectives to respond to stressors, regardless of the stressors' mode of action. We expect that further research will determine whether this form of environmental sensing and adaptation of cell collectives via cell-density increase is common to other biological systems. Interestingly, this idea is in line with recent advancements in the understanding of mechanochemical feedback in development and disease, where local cell density can determine the fates of cell collectives (55). From this perspective, the connection we discovered could represent a primitive example of a collective mechanochemical feedback loop which might be described by the paradigm of MIPS. To this end, the biophysical insights gained may not only offer new biomedical treatment strategies against the rise of antimicrobial resistance but may also contribute to our understanding of development and cell-fate determination.

## Materials and Methods

### Kanamycin gradient assay.

-80°C glycerol stock of *Bacillus subtilis* NCIB 3610 wild-type strain (WT) was streaked on a lysogeny-broth (LB) 1.5% agar plate and grown overnight at 37°C. A single colony was picked from this plate and incubated in 1 ml of liquid LB for 3 h at 37°C. A 4 $\mu$l inoculum from this culture was placed in the center of a 0.5% LB agar plate supplemented with 2% of glycerol and 0.1 mM MnSO4 (LBGM (56)) to favor biofilm formation. A kanamycin diffusive disk (Oxoid™ 30 $\mu$g) was placed on a side of the plate 24 h before inoculation to allow the antibiotic to diffuse at room temperature. The distance between the inoculum and the kanamycin disk was approximately 3.2 cm, and plates were incubated for additional 40 h after inoculation at 30°C. A *Δeps* deletion strain was used as a negative control to compare with the WT biofilms.

### Images of swarming plates

Low magnification images of the plates were acquired with a DSLR D5000 Nikon camera (lens AF-S Micro NIKKOR 40 MM 1.28) in a 30°C incubator. The incubator was covered by black tape to avoid reflections and the illumination was provided by a white LED placed on a side of the plate. Higher magnification images (e.g. of the wrinkles) were taken by an Olympus SZ61 microscope by placing the plates in a dark background with illumination coming from a LED ring attached to the microscope.

313
314 **Quantification of the $P_{tapA}$-*yfp* reporter**
315 Biofilm extracellular matrix production was characterized by using a modified strain carrying $P_{tapA}$-*yfp,* a
316 fluorescence reporter for the expression of *tapA-sipW-tasA* operon. The kanamycin gradient assay was
317 repeated by inoculating this strain in LBGM (1.2% and 2% glycerol) swarming agar plates. The experiment
318 was replicated three times with three different lenses and microscopes: 2x (Nikon Apo Lambda 2x UW, NA
319 0.1), 2x (Nikon Plan 2x UW, NA 0.06), 2.5x (Leica 2.5x N PLAN, NA 0.07); microscopes: two Nikon Eclipse
320 Ti2 and Leica DMi8. Images were taken every half an hour for a period of ~40 h in a region of 3x9 $cm^2$ going
321 from the disk to the inoculum. The images were stitched using the "Grid/Collection stitching" plugin (57) in
322 Fiji (58). The experiment was repeated twice in absence of kanamycin with the first two microscopes and
323 lenses. To calculate the fluorescent signal, a region of interest was drawn in Fiji surrounding the area where
324 the wrinkles appeared. The signal was normalized by subtracting the minimum value of pixel intensity
325 recorded in the timelapse and dividing by the maximum of the signal for each of the microscopes.
326
327 **Raft and islands sizes**
328 The size of the rafts within the swarm were obtained from three different experiments. A freehand line drawn
329 with Fiji/imageJ (58) enclosing the raft was used to measure the area within the line. Measurements across
330 different positions and time points were used to account for the variability in raft size within a swarm
331 depending on the position and/or time after expansion begins (53). To measure the islands size, timelapses of
332 islands formation in presence and absence of kanamycin were used. The first frame (just before islands
333 appeared) was subtracted to the timelapse and then a gaussian filter was applied to remove noise. Finally, the
334 timelapse was threshold and the initial size of the islands was measured by 'regionprops' in Matlab.
335
336 **Characterization of island formation.**
337 We characterized the double layer using 2x (Nikon Plan 2x UW, NA 0.06), 2.5x (Leica 2.5x N PLAN, NA
338 0.07) and 10x (Nikon 10x PLAN FLUOR PH2 DLL, NA 0.3) magnifications in two different microscopes,
339 Nikon Eclipse Ti2 and Leica DMi8. The images were acquired every 2 min in the Nikon Eclipse Ti2 and every
340 1 min in the Leica Dmi8 using brightfield illumination. Cell motility and cell density were recorded with a 40x
341 objective (Nikon 40x LWD, NA 0.55) at 37°C. Cell motility was measured by adapting a Particle Image
342 Velocimetry (PIV) code written in Matlab (59). The surface coverage was measured by thresholding the
343 images and dividing the area covered by bacteria by the total area of our field of view. The threshold was set
344 by using the command 'imbinarize' in Matlab and adapting the sensitivity of its threshold to account for the
345 best estimate of cells in the field of view.
346
347 **Near UV experiments.**
348 Bacteria were irradiated by near UV-Violet light for 30 s using the inverted microscope Dmi8 (Leica
349 Microsystems) and the LED light source, SOLA SM II Light Engine (Lumencor), with an excitation filter
350 400/16 using a 40x objective (Leica 40x PH2 HC PL FLUO, NA 0.6) for approximately 3.5 minutes at an
351 intensity of 1.2 to 5.3 $mW/mm^2$. The light intensities were measured by placing a photodiode power sensor
352 (Thorlabs S120C) on the microscope stage. To irradiate a larger area than the one with the epi-fluorescence
353 set up, a Thorlabs 405 nm light LED was coupled to a cage cube (see Table S1 for details about the components
354 of the set up). The light coming from the LED was concentrated by an aspheric condenser lens and reflected
355 by a $45^o$ dichroic mirror towards the sample. The area illuminated is roughly a circle of 2.5 mm radius at an
356 intensity of 1.5 $mW/mm^2$. The surface coverage was calculated by binarizing the time lapses applying a locally
357 adaptive threshold in Matlab. The sensitivity of such threshold was changed along the time lapse when cell
358 density was rapidly increasing and the same value of the threshold could not account for the total number of
359 particles.
360 The trajectories of the swarming bacteria in the phase diagram were calculated by calculating the $Pe_r$ and the
361 surface coverage as detailed in the previous section. The trajectories are the result of continuous irradiation
362 with either of the setups previously described. When illuminated by the epifluorescence the trajectories were
363 plotted until a jam of bacteria was observed in the field of view. When shining UV from the condenser the

trajectories were plotted until bacteria were completely immotile (Fig. S9). Data for speed and surface coverage of bacteria has been smoothed by the 'smooth' function in Matlab.

**Quorum sensing experiments**

The same protocol as the explained in 'kanamycin gradient assay' was used to proof the swarming behaviour, the formation of islands and the biofilm development of the two quorum-sensing knockout strains: *Δopp* and *Δhprc*. Formation of islands and biofilm images were taken as explained in previous sections.

**Phase diagram.**

To calculate the phase diagram of rotational Péclet number ($Pe_r$) with respect to surface coverage, time-lapses of swarming bacteria coming from 6 different experiments were analysed. The 'jammed bacteria' data plotted in the diagram (Fig. 4a) were calculated by analysing the 4 s of the time lapse prior to jam formation. Videos were acquired at 29-33 fps.

The average speed within the swarm was calculated as described earlier and used to then calculate the $Pe_r$ defined as:

$$Pe_r = \frac{u}{LD_r}$$

Where $u$ is the average cell speed within the swarm for a given time point, $L$ is the aspect ratio of the swarmers calculated to be 3.2 in average and $D_r$ the rotational diffusivity of the bacteria. The rotational diffusivity was estimated by comparing our speeds at surface coverage 0.65 with the speeds of the phase diagram in (32) for the same surface coverage, from which $D_r$ can be obtained as:

$$D_r = \frac{Lu}{Pe_r}$$

This gives $D_r = 0.21 \pm 0.05\ s^{-1}$, from an average of 13 different values from 3 independent experiments. To check whether this result was sensible, we resuspended in water a sample of swarmers from a plate. Then, we recorded a video of these swarmers for 10 s and calculated $D_r$ with a tracking code written in Python (60). $D_r$ was obtained as the gradient of the angular mean-square displacement of the tracks and gave a value of $D_r = 0.35\ s^{-1}$. Although this is slightly higher than the previous result, it should be kept in mind that the former estimate is for cells that are moving on an agar surface, rather than swimming in a bulk fluid.

Notice that, the $Pe_r$ in Damme *et al* (32) is obtained from instantaneous velocities of individual particles. In absence of those, we used an effective $Pe_r$ derived from the local average velocity within the swarm. This is likely to overestimate the value of $Pe_r$ of the experimental points.

**Physical barrier**

A 3% agarose solution in water was autoclaved and then poured in a Petri dish. Once it solidified, a rectangular region (6 x 1 cm) was cut out and vertically placed on a molten swarming liquid LBGM (0.5% agar). Once it solidified, swarming bacteria were inoculated in the centre of the plate. Videos of the formation of islands were recorded under 2x (Nikon Plan 2x UW, NA 0.06) in a Nikon Eclipse Ti2 microscope.

**Biofilm inhibition assay**

4 $\mu$l of the antibiotic kanamycin coming from four different stocks with the next concentrations: 50, 37.5, 25 and 12.5 $\mu$g/$\mu$l were added to four different diffusive disks. These diffusive disks were placed on a side of LBGM 0.5% agar plate for 24 h. After bacteria inoculation, the plates were incubated in a 30°C incubator for roughly 5 h until the swarming front halted. Then, additional 4 $\mu$l of the next stock concentrations of kanamycin were added to the initial ones: 0, 12.5, 25 and 37.5 $\mu$g/$\mu$l so the total amount of kanamycin administered was kept constant and equal to 200 $\mu$g.

**Wrinkle wavelength quantification**

To measure the wavelength of the wrinkles we calculated the interdistance of nearest parallel wrinkles. When this was not possible, the wavelength was estimated by calculating the autocorrelation function of image intensity in space using a Fiji macro made by Michael Schmid

(https://imagej.nih.gov/ij/macros/RadiallyAveragedAutocorrelation.txt) (2008) and then fitting the decay of that function to a double exponential of the form:

$$f(x) = ae^{bx} + ce^{dx}.$$

Here, the two characteristic wavelengths (1/b and 1/d) correspond to the image noise and the actual wrinkle wavelength respectively.

**Statistics**

Data are reported as Mean±s.e.m. calculated from at least 3 independent experiments unless otherwise indicated.

**References**


1. Bleuven C, Landry CR (2016) Molecular and cellular bases of adaptation to a changing environment in microorganisms. *Proc R Soc B Biol Sci* 283(1841):20161458.
2. Crabbé A, Jensen PØ, Bjarnsholt T, Coenye T (2019) Antimicrobial Tolerance and Metabolic Adaptations in Microbial Biofilms. *Trends Microbiol* 27(10):850–863.
3. Young JW, Locke JCW, Elowitz MB (2013) Rate of environmental change determines stress response specificity. *Proc Natl Acad Sci* 110(10):4140–4145.
4. Hanke ML, Kielian T (2012) Deciphering mechanisms of staphylococcal biofilm evasion of host immunity. *Front Cell Infect Microbiol* 2(May):62.
5. Bridier A, Briandet R, Thomas V, Dubois-Brissonnet F (2011) Resistance of bacterial biofilms to disinfectants: a review. *Biofouling* 27(9):1017–1032.
6. Lories B, et al. (2020) Biofilm Bacteria Use Stress Responses to Detect and Respond to Competitors. *Curr Biol* 30(7):1231-1244.e4.
7. Meredith HR, Srimani JK, Lee AJ, Lopatkin AJ, You L (2015) Collective antibiotic tolerance: Mechanisms, dynamics and intervention. *Nat Chem Biol* 11(3):182–188.
8. Flemming H-C, Wingender J (2010) The biofilm matrix. *Nat Rev Microbiol* 8(9):623–33.
9. Liu J, et al. (2015) Metabolic co-dependence gives rise to collective oscillations within biofilms. *Nature* 523(7562):550–4.
10. Costerton JW (1999) Bacterial Biofilms: A Common Cause of Persistent Infections. *Science* 284(5418):1318–1322.
11. Epstein AK, Pokroy B, Seminara A, Aizenberg J (2011) Bacterial biofilm shows persistent resistance to liquid wetting and gas penetration. *Proc Natl Acad Sci* 108(3):995–1000.
12. Vlamakis H, Chai Y, Beauregard P, Losick R, Kolter R (2013) Sticking together: building a biofilm the Bacillus subtilis way. *Nat Rev Microbiol* 11(3):157–68.
13. Hoffman LR, et al. (2005) Aminoglycoside antibiotics induce bacterial biofilm formation. *Nature* 436(7054):1171–1175.
14. Wang Y, et al. (2011) Phenazine-1-carboxylic acid promotes bacterial biofilm development via ferrous iron acquisition. *J Bacteriol* 193(14):3606–3617.
15. Zhang W, et al. (2014) Nutrient depletion in Bacillus subtilis biofilms triggers matrix production. *New J Phys* 16(1):015028.
16. Chu EK, Kilic O, Cho H, Groisman A, Levchenko A (2018) Self-induced mechanical stress can trigger biofilm formation in uropathogenic Escherichia coli. *Nat Commun* 9(1). doi:10.1038/s41467-018-06552-z.
17. Bhattacharyya S, Walker DM, Harshey RM (2020) Necrosignaling: Cell death triggers antibiotic survival pathways in bacterial swarms. *bioRxiv*:2020.02.26.966986.
18. Lai S, Tremblay J, Déziel E (2009) Swarming motility: A multicellular behaviour conferring antimicrobial resistance. *Environ Microbiol* 11(1):126–136.
19. Butler MT, Wang Q, Harshey RM (2010) Cell density and mobility protect swarming bacteria against antibiotics. *Proc Natl Acad Sci* 107(8):3776–3781.
20. Kearns DB (2010) A field guide to bacterial swarming motility. *Nat Rev Microbiol* 8(9):634–644.
21. Rosenthal K, Oehling V, Dusny C, Schmid A (2017) Beyond the bulk: Disclosing the life of single microbial cells. *FEMS Microbiol Rev* 41(6):751–780.
22. Dufrêne YF, Persat A (2020) Mechanomicrobiology: how bacteria sense and respond to forces. *Nat Rev Microbiol* 18(4):227–240.
23. Stewart PS (2014) Biophysics of biofilm infection. *Pathog Dis* 70(3):212–218.

24. Hol FJH, Hubert B, Dekker C, Keymer JE (2015) Density-dependent adaptive resistance allows swimming bacteria to colonize an antibiotic gradient. *ISME J* 2:1–9.
25. Vicsek T, Czirók A, Ben-Jacob E, Cohen I, Shochet O (1995) Novel Type of Phase Transition in a System of Self-Driven Particles. *Phys Rev Lett* 75(6):1226–1229.
26. Bechinger C, et al. (2016) Active Particles in Complex and Crowded Environments. *Rev Mod Phys* 88(4):045006.
27. Geyer D, Martin D, Tailleur J, Bartolo D (2019) Freezing a Flock: Motility-Induced Phase Separation in Polar Active Liquids. *Phys Rev X* 9(3):031043.
28. Gonnella G, Marenduzzo D, Suma A, Tiribocchi A (2015) Motility-induced phase separation and coarsening in active matter. *Elsevier Masson SAS* 16(3):316–331.
29. Barré J, Chétrite R, Muratori M, Peruani F (2015) Motility-Induced Phase Separation of Active Particles in the Presence of Velocity Alignment. *J Stat Phys* 158(3):589–600.
30. Liu G, et al. (2019) Self-Driven Phase Transitions Drive Myxococcus xanthus Fruiting Body Formation. *Phys Rev Lett* 122(24):248102.
31. Digregorio P, et al. (2018) Full Phase Diagram of Active Brownian Disks : From Melting to Motility-Induced Phase Separation. *Phys Rev Lett* 121(9):98003.
32. van Damme R, Rodenburg J, van Roij R, Dijkstra M (2019) Interparticle torques suppress motility-induced phase separation for rodlike particles. *J Chem Phys* 150(16):164501.
33. Cates ME, Tailleur J (2015) Motility-Induced Phase Separation. *Annu Rev Condens Matter Phys* 6(1):219–244.
34. Cates ME, Marenduzzo D, Pagonabarraga I, Tailleur J (2010) Arrested phase separation in reproducing bacteria creates a generic route to pattern formation. *Proc Natl Acad Sci* 107(26):11715–11720.
35. Asally M, et al. (2012) Localized cell death focuses mechanical forces during 3D patterning in a biofilm. *Proc Natl Acad Sci* 109(46):18891–6.
36. Ghosh P, Ben-Jacob E, Levine H (2013) Modeling cell-death patterning during biofilm formation. *Phys Biol* 10(6):066006.
37. Cairns LS, Hobley L, Stanley-Wall NR (2014) Biofilm formation by Bacillus subtilis: new insights into regulatory strategies and assembly mechanisms. *Mol Microbiol* 93(4):587–598.
38. Yan J, et al. (2019) Mechanical instability and interfacial energy drive biofilm morphogenesis. *Elife* 8:1–28.
39. Kesel S, et al. (2016) Direct Comparison of Physical Properties of Bacillus subtilis NCIB. *Appl Environ Microbiol* 82(8):2424–2432.
40. Nagórska K, Ostrowski A, Hinc K, Holland IB, Obuchowski M (2010) Importance ofeps genes fromBacillus subtilis in biofilm formation and swarming. *J Appl Genet* 51(3):369–381.
41. Vlamakis H, Aguilar C, Losick R, Kolter R (2008) Control of cell fate by the formation of an architecturally complex bacterial community. *Genes Dev* 22(7):945–953.
42. Peruani F, Klauss T, Deutsch A, Voss-Boehme A (2011) Traffic Jams, Gliders, and Bands in the Quest for Collective Motion of Self-Propelled Particles. *Phys Rev Lett* 106(12):128101.
43. Weitz S, Deutsch A, Peruani F (2015) Self-propelled rods exhibit a phase-separated state characterized by the presence of active stresses and the ejection of polar clusters. *Phys Rev E* 92(1):012322.
44. Qiu F, et al. (2001) Spinodal decomposition of a binary fluid with fixed impurities. *J Chem Phys* 115(8):3779–3784.
45. Bartolini A, et al. (2019) Liquid-liquid phase separation of polymeric microdomains with tunable inner morphology: Mechanistic insights and applications. *J Colloid Interface Sci* 556:74–82.
46. Su PT, et al. (2012) Bacterial Colony from Two-Dimensional Division to Three-Dimensional Development. *PLoS One* 7(11):1–10.
47. Grant MAA, Waclaw B, Allen RJ, Cicuta P (2014) The role of mechanical forces in the planar-to-bulk transition in growing Escherichia coli microcolonies. *J R Soc Interface* 11(97). doi:10.1098/rsif.2014.0400.
48. Yang J, Arratia PE, Patteson AE, Gopinath A (2019) Quenching active swarms: effects of light exposure on collective motility in swarming Serratia marcescens. *J R Soc Interface* 16(156):20180960.
49. Krasnopeeva E, Lo CJ, Pilizota T (2019) Single-Cell Bacterial Electrophysiology Reveals Mechanisms of Stress-Induced Damage. *Biophys J* 116(12):2390–2399.
50. Frangipane G, et al. (2018) Dynamic density shaping of photokinetic E. Coli. *Elife* 7:1–14.

51. Arlt J, Martinez VA, Dawson A, Pilizota T, Poon WCK (2018) Painting with light-powered bacteria. *Nat Commun* 9(1):768.
52. Cates ME (2012) Diffusive transport without detailed balance in motile bacteria: does microbiology need statistical physics? *Reports Prog Phys* 75(4):42601.
53. Jeckel H, et al. (2019) Learning the space-time phase diagram of bacterial swarm expansion. *Proc Natl Acad Sci* 116(5):1489–1494.
54. Be'er A, Ariel G (2019) A statistical physics view of swarming bacteria. *Mov Ecol* 7(1). doi:10.1186/s40462-019-0153-9.
55. Hannezo E, Heisenberg C-P (2019) Mechanochemical Feedback Loops in Development and Disease. *Cell* 178(1):12–25.
56. Shemesh M, Chai Y (2013) A combination of glycerol and manganese promotes biofilm formation in Bacillus subtilis via histidine kinase KinD signaling. *J Bacteriol* 195(12):2747–54.
57. Preibisch S, Saalfeld S, Tomancak P (2009) Globally optimal stitching of tiled 3D microscopic image acquisitions. *Bioinformatics*. doi:10.1093/bioinformatics/btp184.
58. Schindelin J, et al. (2012) Fiji: an open-source platform for biological-image analysis. *Nat Methods* 9(7):676–82.
59. Sveen JK (2004) *An introduction to MatPIV v. 1.6.1*.
60. Mosby LS, Polin M, Köster DV (2020) A Python based automated tracking routine for myosin II filaments. *J Phys D Appl Phys*. doi:10.1088/1361-6463/ab87bf.

**Acknowledgements**

This research is funded by the MRC Doctoral Training Partnership (MR/N014294/1). MP and MA acknowledge support from EPSRC grant, Bridging the Gaps initiative (EP/M027503/1). MA acknowledges BBSRC/EPSRC grant to the Warwick Integrative Synthetic Biology Centre (BB/M017982/1). We thank Lewis Mosby for his help with estimates of the rotational diffusivity, and Drs. Darius Köster and Meera Unnkrishnan for their comments to the manuscript.

555 **Figures**

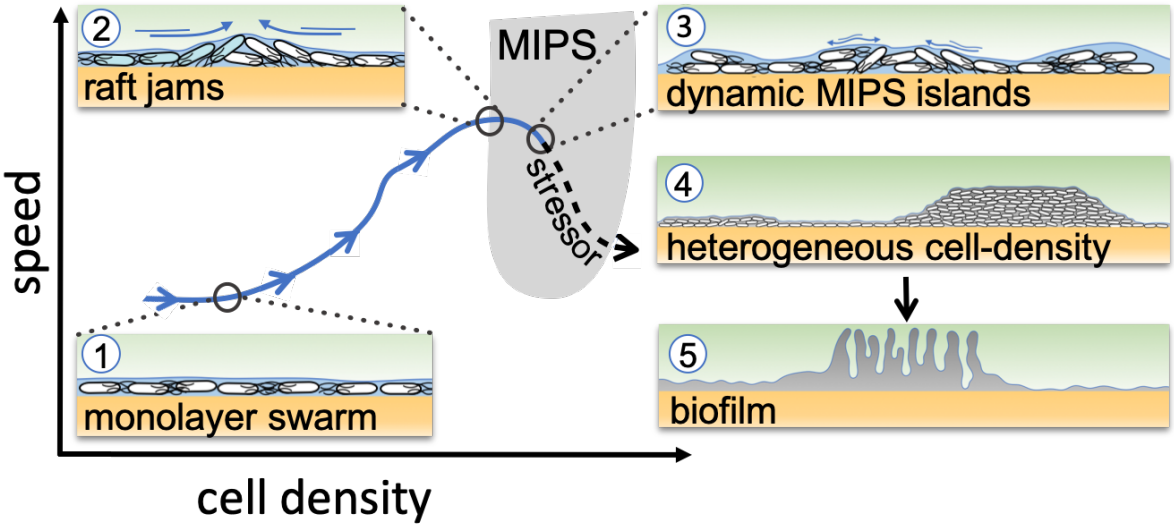


556

557 **Figure 1. Schematic of the transition from swarming to biofilm formation through MIPS.** *B. subtilis* cells
558 swarm in a monolayer (stage 1). As cell density increases, cells form fast-moving rafts which can collide and
559 form transient jams. Cells at the boundary between the colliding rafts are pushed upwards and protrude from
560 the surrounding monolayer (stage 2). Further increase in surface coverage can promote the formation of
561 dynamic MIPS-like islands where cells accumulate within the swarm while still being dynamic (stage 3).
562 Eventually, this uneven distribution of cell density gives rise to macroscopic spatial cell-density heterogeneity
563 in cell density (stage 4), which can lead to the formation of biofilms (stage 5).

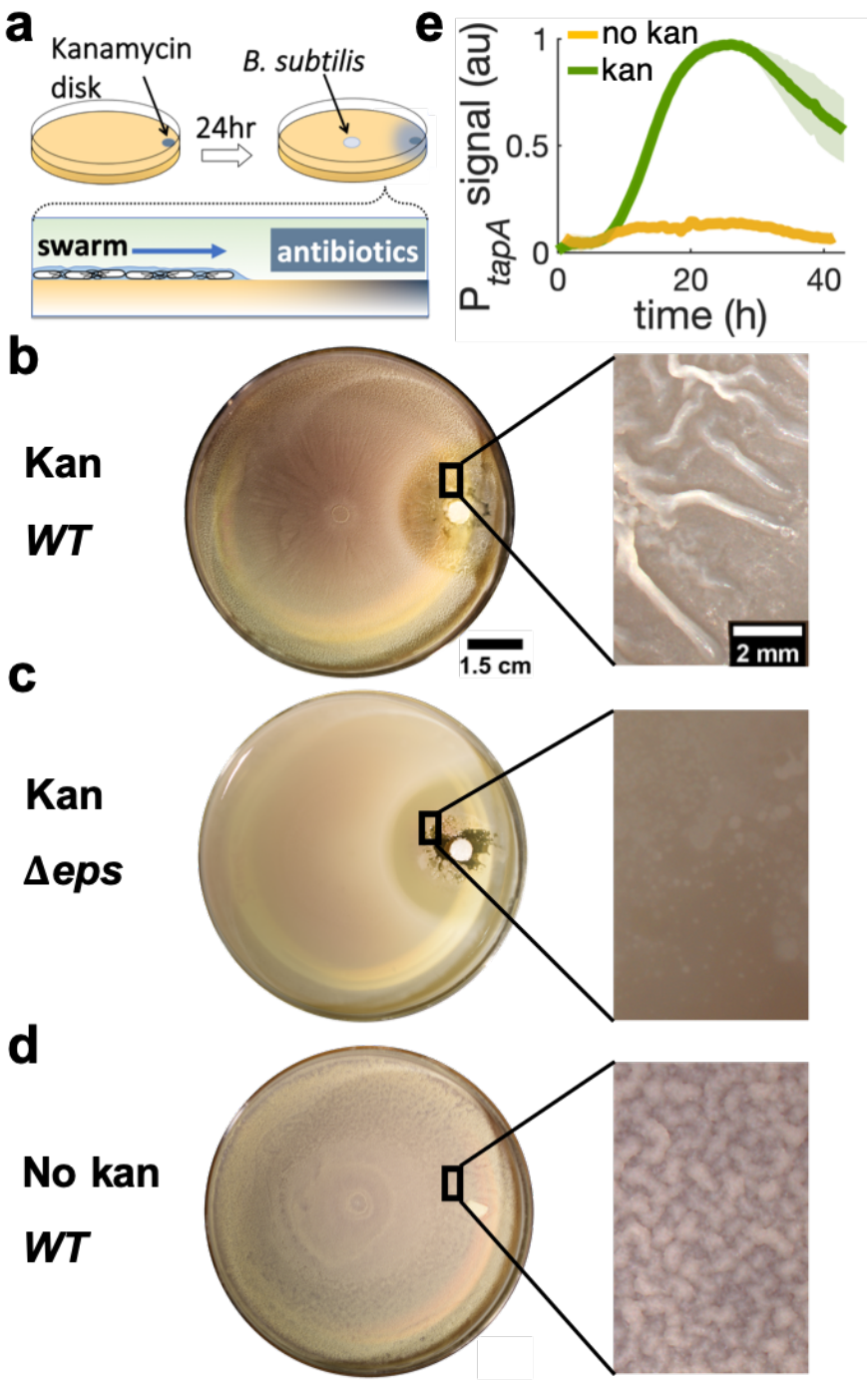


**Figure 2. Swarming cells transit into biofilm in presence of kanamycin gradient.**

a) Schematics of swarming bacteria expanding from the center of a 9 cm Petri dish towards a kanamycin diffusive disk. Kanamycin disk was placed for 24 hours to form a spatial gradient (Fig. S1). b, c, d) Swarming *B. subtilis* plates after 40h incubation. Wrinkles are formed at the region ~2 cm away from disk with b) wildtype (WT), but not with c) *Δ*eps deletion strain. d) WT swarming plate with a diffusive disk without antibiotics. Zoomed images show the colony surface. e) Mean fluorescence intensity of $P_{tapA}$-*yfp* for the front of the plate in presence (green) and absence of kanamycin (yellow). The mean was taken from three independent experiments in the kanamycin case and two independent experiments in absence of kanamycin. The shady areas represent the s.e.m.

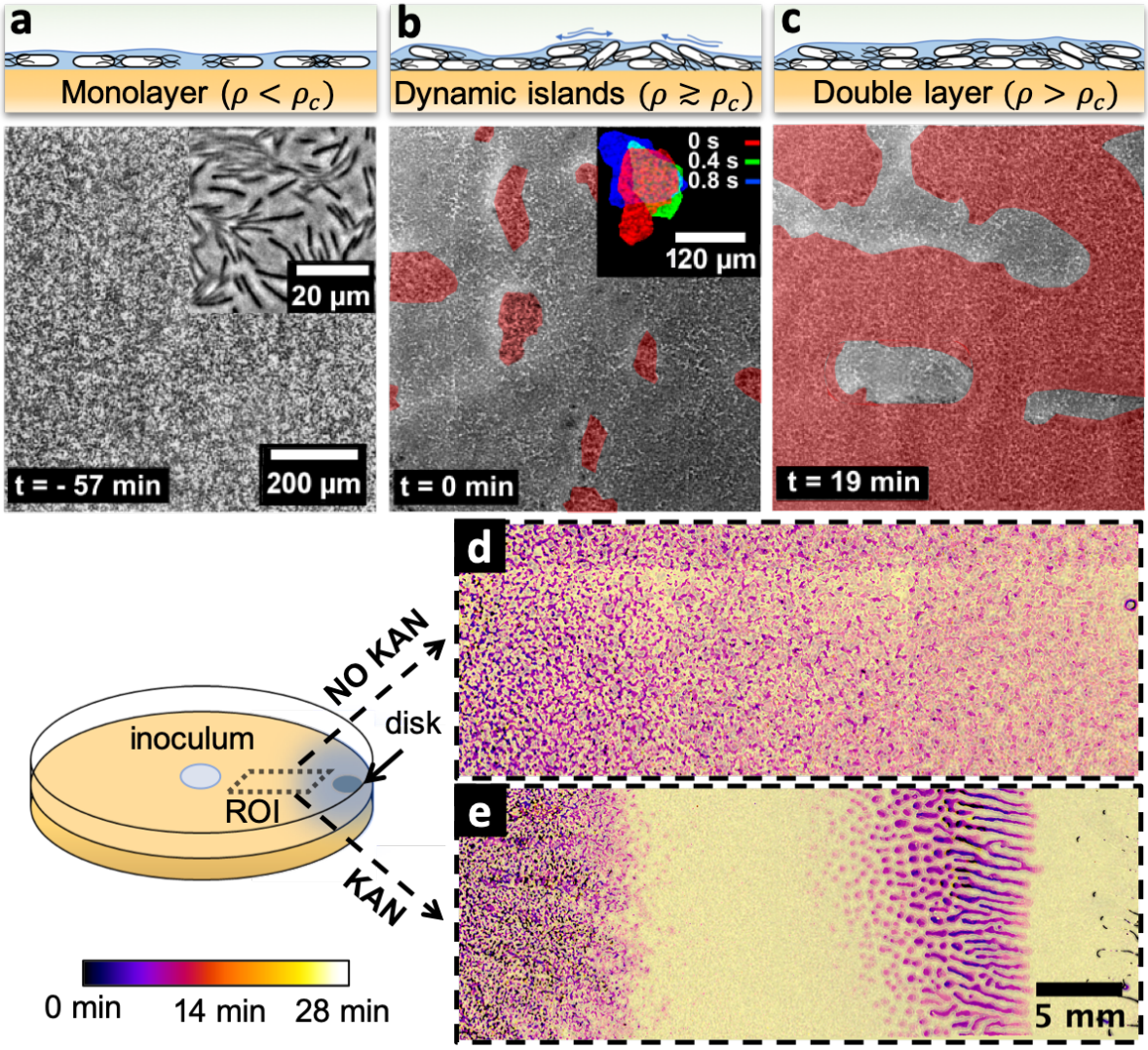


**Figure 3. Swarming bacteria form patterned multi-layer regions in presence of kanamycin.**

a, b, c) Microscopy images of swarming bacteria and side-view illustrations at different levels of cell density ($\rho$). Timestamp is relative to the formation of dynamic multi-layer islands. a) When cell density is below a threshold $\rho_c$, cells swarm in a monolayer. Image is 57 minutes prior to islands formation. Inset is a zoomed image showing swarming rafts. b) Increase in cell density leads to formation of second layers, highlighted in pseudo red. These islands are highly dynamic, and cells are motile. The shape of the islands changes dynamically within one second (insert). See also Supplementary Video 4. c) Over time, the islands increase their size and merge together to double-layered regions (shown in red), coexisting with mono-layered regions. Double layered regions are seen darker than mono layered regions. d, e) Images of swarming colony with and without kanamycin. Diagram illustrates the regions of interest (ROI) used for panels. The dynamics of island formation are colour coded using the lookup table. The origin of times is the appearance of island. See also Supplementary Video 6. d) In the absence of kanamycin, multilayer regions are much grainer with no clear patterns of propagation. e) In the presence of kanamycin, multi-layered regions have a defined pattern, starting from the regions closer to kanamycin to form an elongated shape. These regions appear predominantly at ~7 mm away from kanamycin.

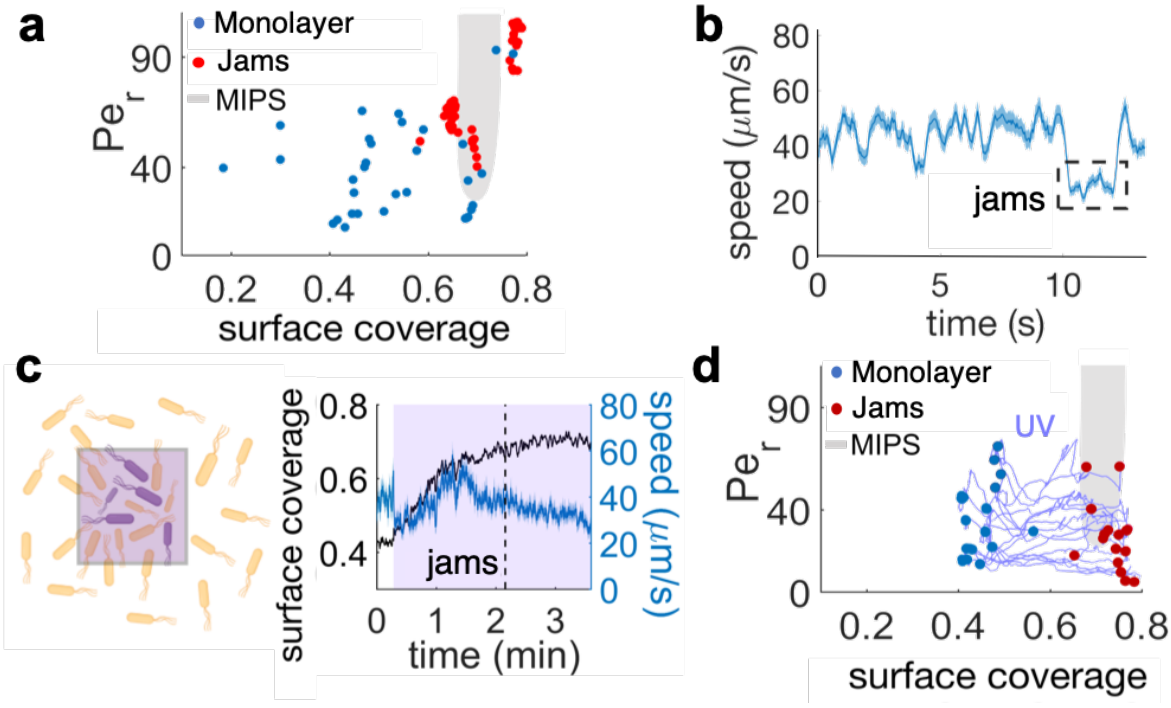


**Figure 4. The interplay between cell density and cell speed primes jamming and multi-layer formation.**

a) Phase diagram of surface coverage and the rotational Peclet number ($P_{e_r}$). $P_{e_r}$ is proportional to the cell motility speed (see Methods). Greyed region depicts motility-induced phase separation (MIPS) heterogeneity. Each data point represents a result of a 4-sec single-cell time-lapse microscopy data. The time-lapse data in which jamming events are observed are shown in red (see Supplementary Video 3). Jams appear exclusively under the condition near the border of MIPS region. b) The speed of motile cells drops by half during jamming (highlighted by dashed rectangle). Increase in jamming events lead to formation of islands (see Fig.2 and Supplementary Video 4). c, left) Illustrative diagram showing the accumulation of cells by UV irradiation. Cell speeds drop within the irradiated region (show by purple square), which elevates the surface coverage. c, right) UV irradiation elevates surface coverage. Graph shows the dynamics of surface coverage (black) and cell speed (cyan). Magenta is the period with UV light illumination (1.2 mW/mm$^2$). Vertical dashed line shows a jamming event. d) Time evolution trajectories of surface coverage and rotational Peclet number with UV illumination experiment. Blue dots are before UV illumination and red dots are when jams appear. Increasing surface coverage by UV induces formation of jams at the border to MIPS region (grey).

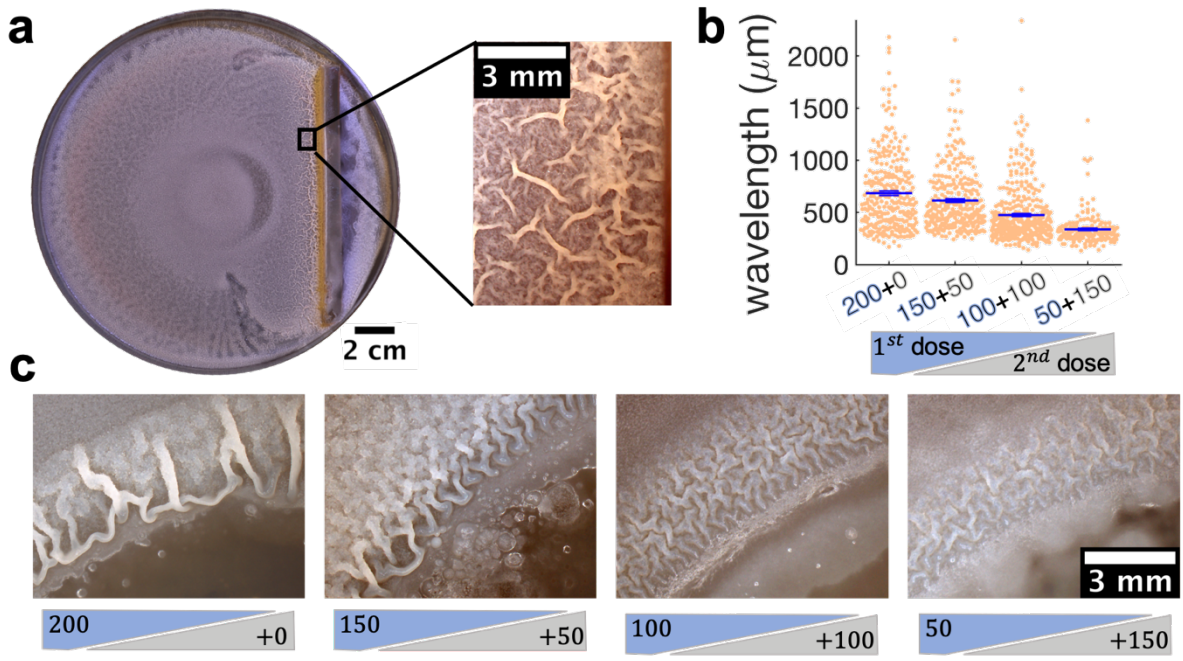


**Figure 5. Locally increasing cell density is sufficient in inducing wrinkle formation, which can be inhibited by sequential administration of kanamycin**.

a) A physical barrier placed on agar triggers wrinkle formation. Wrinkles are formed at the region close to the barrier. A plate was incubated for 40 hours as in Figure 1. b, c) Kanamycin was sequentially administered in two different doses to a disk while keeping the total to be 200 $\mu g$. The first administration was added as in other experiments, while the second was added to the disk when the islands were about to appear. b) The wavelengths of wrinkles with respect to the doses of first (blue font) and second (gray font) administrations ($\mu g$). c) Microscopy images of wrinkles induced by kanamycin. The first dose is in the blue shade and the second dose in the grey shade. Even when the total dose is kept the same, equal or greater 2$^{nd}$ dose inhibits biofilm formation.

**Supplementary Information**

# Bacterial swarms undergo localized dynamic phase transition to form antibiotic-induced biofilms

**Authors**
Iago Grobas[1], Marco Polin[1,2,3,*†] & Munehiro Asally[4,5,6,*†]

**Affiliations**
[1]Warwick Medical School, University of Warwick, Coventry, CV4 7AL, United Kingdom
[2]Centre for Mechanochemical Cell Biology, University of Warwick, Coventry, CV4 7AL, United Kingdom
[3]Physics Department, University of Warwick, Coventry, CV4 7AL, United Kingdom
[4]Bio-Electrical Engineering Innovation Hub, University of Warwick, Coventry, CV4 7AL, United Kingdom
[5]Warwick Integrative Synthetic Biology Centre, University of Warwick, Coventry, CV4 7AL, United Kingdom
[6]School of Life Sciences, University of Warwick, Coventry, CV4 7AL, United Kingdom
†equal contribution
*Correspondence should be addressed to MP (m.polin@warwick.ac.uk) or MA (m.asally@warwick.ac.uk).

## Materials and Methods

### Calculation of the Minimum Inhibitory Concentration (MIC)

A single colony of *Bacillus subtilis* was incubated in 1 ml LB overnight in a shaking incubator at 37 °C. The OD was measured 18h later and the culture was diluted down to an OD of 0.0085 and incubated for 18h in 5 concentrations of kanamycin from 1 to 5 ug/ml. The MIC was determined as the minimum concentration at which growth was not observed in the liquid culture. Each well plate had 5 replicates and the experiment was repeated at least 3 times for each concentration.

### Roughness measurements for wrinkles

A line of width 50 pixels was drawn over the wrinkles and then the intensity profile was extracted by using 'Plot profile' in ImageJ. The roughness of the profile was defined as:

$$roughness = \frac{\sum_i^N |I_i - \bar{I}|}{N}$$

Where $I$ is the pixel intensity in the profile, $\bar{I}$ is the mean of the profile obtained using the 'smooth' function in Matlab and $N$, the total number of points in the profile.

### Estimation of the kanamycin profile on the swarming plate

The concentration profile of the kanamycin in the plate (Fig.S1) was characterized by using a variation of the Kirby-Bauer assay (1). 800 $\mu$l of a 7 h bacteria culture was inoculated in 3 plates containing LB with 1.5% agar. Then, 3 diffusive disks containing 7.5, 15 or 30 $\mu$g of kanamycin was placed on the surface of each LB agar media. After an incubation of 24 h at 37ºC, we measured the width of the clearance region around the disks. This was used to make a calibration curve relating the amount of kanamycin in the disk and the size of the clearance region. Then, to measure the kanamycin profile in our swarming assay, 6 small pads of agar were cut out of a plate where a kanamycin diffusive disk had been placed 24 h before. These agar pads were placed on top of a confluent plate of WT *B. subtilis* and incubated overnight at 37ºC. We then measured the clearance around these pads and the equivalence to the kanamycin concentration was calculated with the calibration curve. The whole process was repeated to characterize the profile of kanamycin after 40 h of inoculation.

### Quantification of the speed at the swarming front.

To calculate the speed at the swarming edge (Fig. S2), the position of the front closest to the diffusive disk was recorded over time with a DSLR camera (Nikon D5300; lens AF-S Micro NIKKOR 40 MM 1.28) at 37°C. Consecutive front positions were subtracted to highlight the position of the front. This was then used to estimate the front's speed on both the kanamycin side and the opposite side of the agar pad using the inter-frame time of 5 min. From these timelapses we also extracted the distance at which the swarming front halts from the kanamycin disk.

### Multilayer formation within the swarm

To investigate the spatial difference in multilayer formation throughout the swarm, videos of the bacteria were taken at 2x magnification and 0.017 fps, for 2h at 30 ºC (Supplementary Video 6). The videos were acquired following a tiling of the rectangular region from the diffusive disk to the opposite end of the plate, with 12 sectors along the diameter and 5 across. The videos were then stitched together using the "Grid/Collection stitching" plugin (2) in Fiji. To enhance the contrast of the different layers, the frame just before the multilayer appeared was subtracted from the rest of the time-lapse. The different layers appearing in the swarm were counted for four different positions and they were identified by a local increase in grey value in a wide area of the swarm (Fig. S7). After the 4$^{th}$ layer, the

increase in grey value could not be further identified. Time is measured from the onset of the first islands within the field of view.

**Distance from wrinkles to kanamycin disks of different concentration**

To characterize how the distance between the kanamycin disk and the wrinkles depends on the initial antibiotic concentration within the disk (Fig. S4), diffusive disks containing 30, 100 and 200 $\mu$g of kanamycin were placed on 2-3% glycerol LBGM agar plates. To create the disks, Whatman® filter paper was punched with a hole puncher (diameter 7 mm) and imbibed with 0.6, 2 or 4 $\mu$l of a 50 $\mu$g/$\mu$l kanamycin solution in water. The minimum distance between the kanamycin disk and the nearest wrinkles was measured in 6 different experiments for 30 $\mu$g and 200 $\mu$g of antibiotic and one experiment for 100 $\mu$g.

**Biofilm formation in solid agar near the kanamycin**

To check whether wrinkle formation was promoted also in absence of motility near the kanamycin diffusive disk, the kanamycin diffusive assay was repeated in 1.5% agar. To do so, a kanamycin diffusive disk was place at the center of the solid agar LBGM (2% glycerol) plate. 24h later, a single colony of B. subtilis was incubated in 5 ml of LB for 3h. After that, 500 ul of the culture were spread in the solid agar plates and then incubated for 40 h at 30$^{o}$C.

**Measuring the width of the band where wrinkles appear**

The width of the band where wrinkles appeared around the kanamycin disk was measured for three independent experiments using 30 and 200 $\mu$g of kanamycin. The width was determined by drawing a line across the band where the wrinkles appeared.

**SUPPLEMENTARY FIGURES**

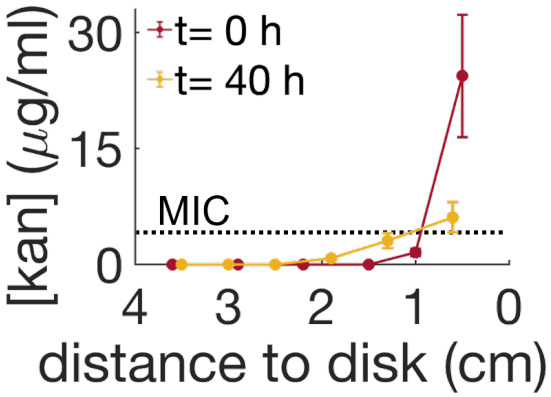


**Figure S1**. **Evolution of the kanamycin profile along the plate in 40 h measured from the kanamycin disk.** The initial profile was made by placing a kanamycin diffusive disk for 24 h on the swarming agar plate. At this point bacteria were inoculated in the center of the plate (t = 0 h). The kanamycin concentration was measured again 40 h later to check the evolution of the gradient with time. The MIC for *B. subtilis* (5 μg/ml) has been indicated with a dotted line. Data obtained from a single experiment.

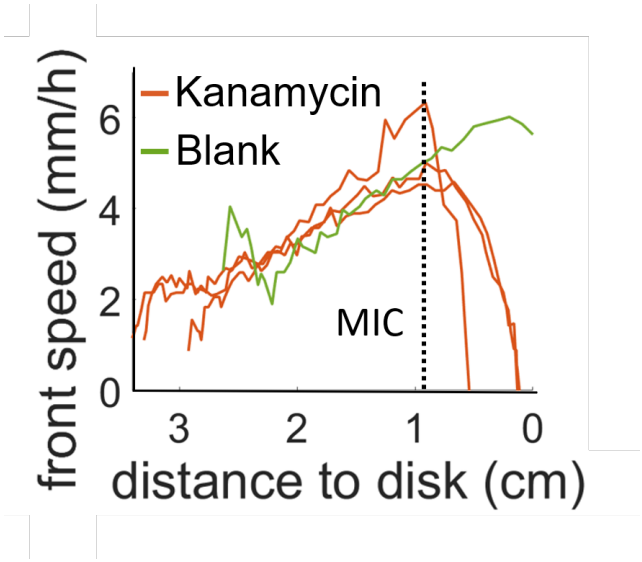


**Figure S2. Speed of the swarming front when approaching to the diffusive disk.** In presence of antibiotic the front speed rapidly decays to then halt completely before it reaches the disk. When a blank disk is placed the swarm invades the whole plate and not decay in speed is observed. The position which corresponds to the MIC (dotted line) was calculated by looking at the position of the MIC line in Fig. S1 for t = 0 h.

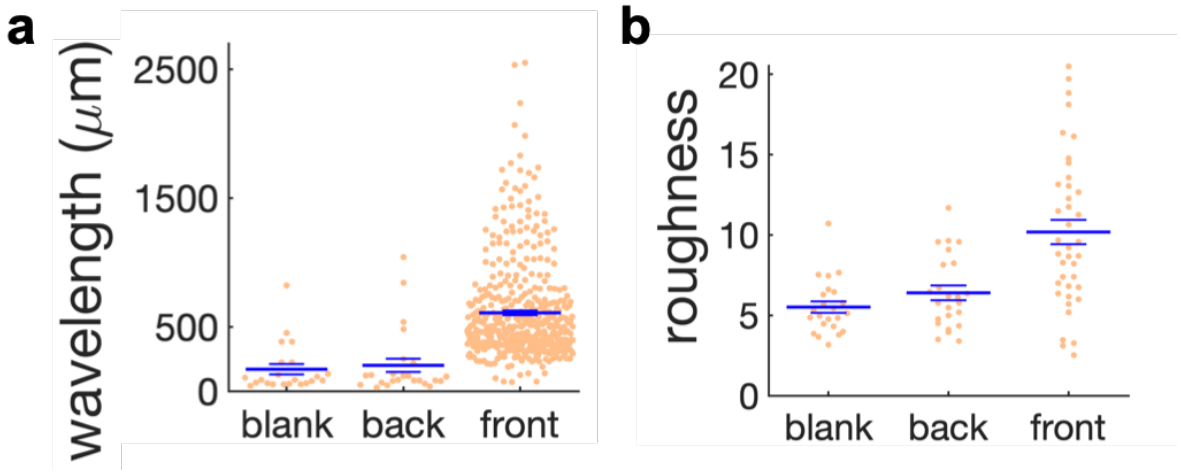


**Figure S3. Quantification of wrinkle formation for different regions in the kanamycin plate and in the blank case.** a) Scatter plot of the wavelength of the wrinkles near the kanamycin disk (front), in the bulk of the plate (back) and in absence of kanamycin (blank). b) Scatter plot of the roughness of the wrinkles in the same regions than for the wavelength. The large horizontal line shows the mean of the distributions and the small bars the sem.

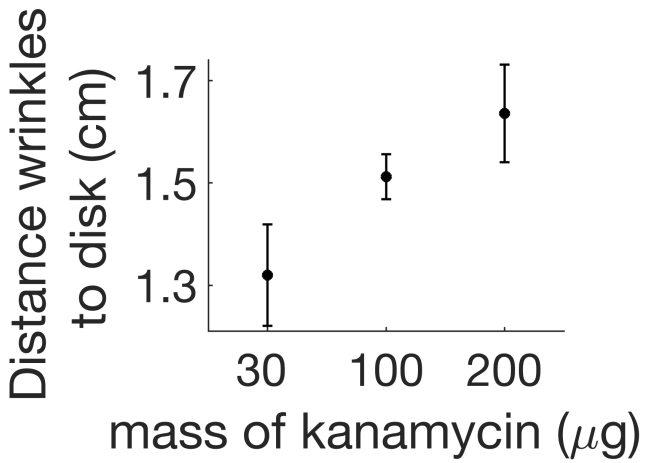


**Figure S4. Distance where the wrinkles appear depending on the amount of kanamycin in the diffusive disk**. The wrinkles appear further from the kanamycin disk with increasing concentration of the antibiotic. The data for 100 ug comes from a single experiment. Data for 30 and 200 ug come at least from three different replicates.

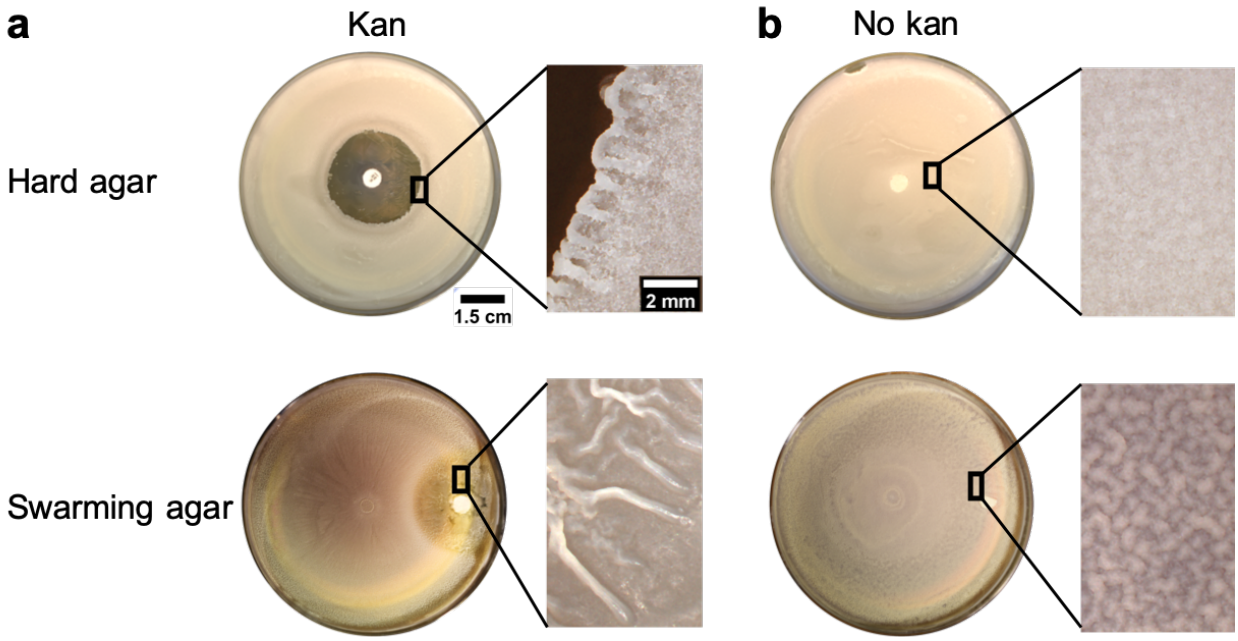


**Figure S5. Comparison of wrinkle formation between hard agar and swarming agar in presence of a gradient of kanamycin.** a) Weak wrinkles appeared at the edges of the clearance zone made by kanamycin for the hard agar case in comparison to the swarming agar case. b) In the blank disk case there is a slight surface roughness and wrinkles are not formed in hard agar or weakly formed in swarming agar.

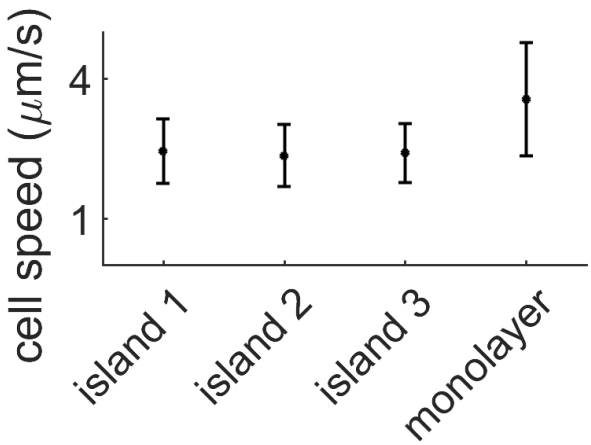


**Figure S6. Average speed in the monolayer vs speed within the island**. The average cell speed of the swarm was measured with PIV for 3 different multi-layered regions and for the monolayer surrounding them. The speed in the monolayer is almost double the multilayer case. Data comes from a single replicate.

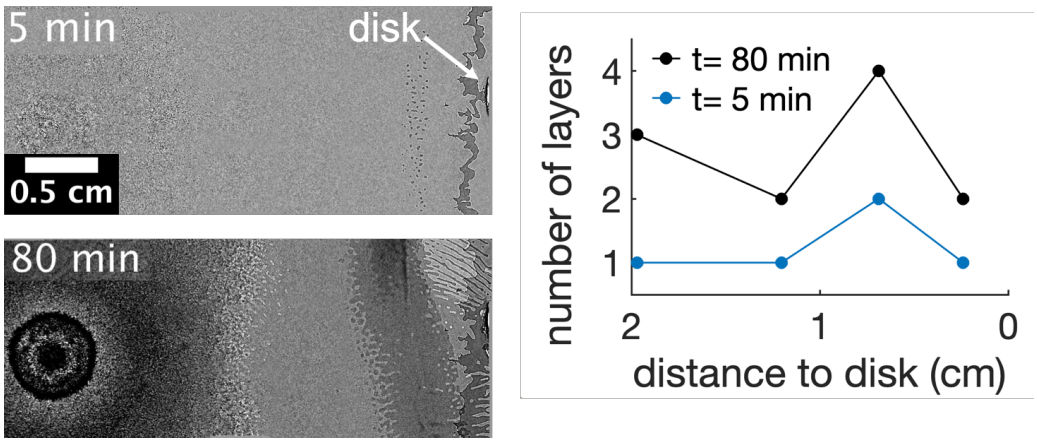


**Figure S7. Asymmetric multilayer formation along time in presence of kanamycin.** The multilayer starts 0.7 cm away from the kanamycin disk. The formation of these islands marks where the multilayer first develops. Here, the number of layers continuously increases but it does not spread towards the center of the swarm giving rise to a gap in cell density between the swarming front and the center. The number of layers were measured by the number of times that a darker layer could be observed in the field of view. The origin of times is when the first island is seen in the field of view. Data taken from a single replicate.

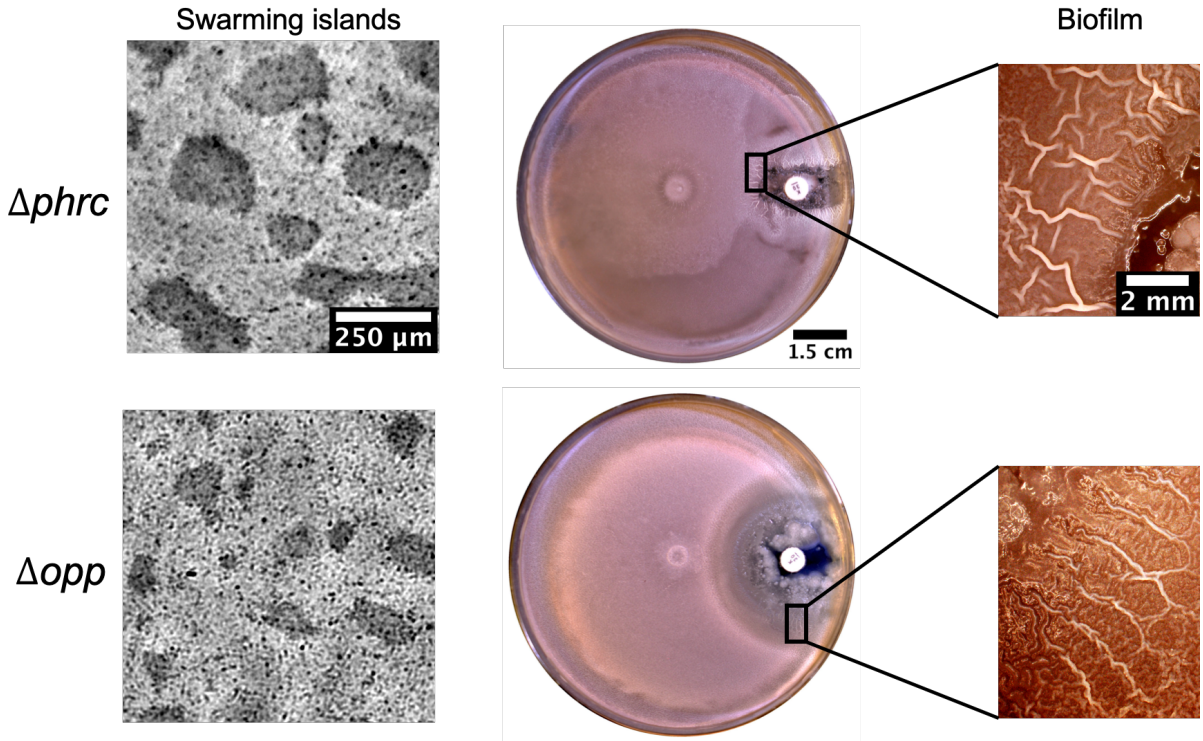


**Figure S8. Islands and posterior wrinkle formation in presence of a kanamycin gradient by the quorum sensing knock out strains Δ*phrc* and Δ*opp*.** For both mutants the islands and the wrinkles were formed as in WT. The smaller clearance zone around kanamycin in the *Δphrc* case is due to its genetic resistance to neomycin.

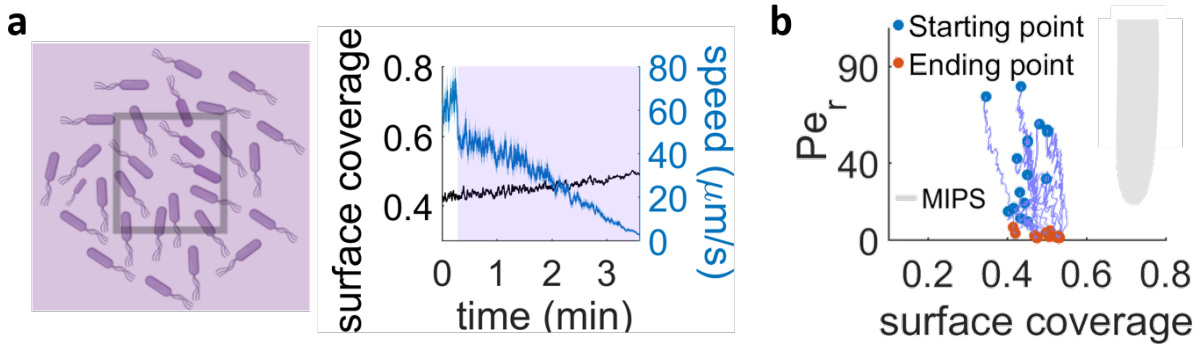


**Figure S9. Exposure with UV light to an area much larger than the field of view.** a) When a region approximately four times larger than our field of view is irradiated, the surface coverage stays nearly constant and we can see a drop in cell speed over time. b) Trajectories in the phase diagram for bacteria continuously irradiated with this set up. The trajectories just decrease their cell velocity and hence they never approach the MIPS region.

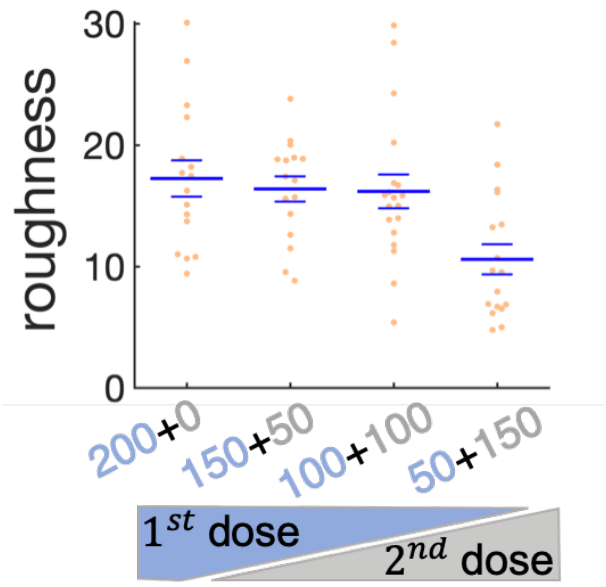


**Figure S10. Effect of sequential administration of kanamycin in wrinkles' roughness.** Scatter plot for the roughness of the wrinkles when the kanamycin dose is split in two times. The first dose of kanamycin is in blue and the second dose in gray. The large bars are the mean of the roughness and the small bars are the sem.

## SUPPLEMENTARY TABLES

**Table 1.** Items used to build the set-up which was used to irradiate a wide area of bacteria. All the components were bought from Thorlabs.

| Item | Model | Specifications |
|---|---|---|
| **Mounted LED** | M405L4 | 405 nm, 1000 mW |
| **Aspheric Condenser Lenses** | ACL25416U-B | Ø1", f = 16.0 mm |
| **25mm SPUTTERED EDGEPASS FILTER** | FELH0450 | Longpass 450 nm |
| **Retaining Ring** | CMRR | C-Mount (1.00"-32) |
| **Cage cube** | Cm1-dch | Dichroic Filter Mount |
| **Adapter** | Sm1a9 | External C-Mount Threads and Internal SM1 Threads |
| **Leica DMI Microscope Camera Port Adapter** | Sm1a50 | Internal SM1 Threads, External SM2 Threads |
| **Coupler, External Threads** | Sm1t2 | 0.5" Long |
| **Adapter** | Sm1a10 | External SM1 Threads and Internal C-Mount Threads |

**Table 2.** List of strains used in this study.

| Strain | Genotype | Source | ID number |
|---|---|---|---|
| **Wild Type** | *B. subtilis* NCIB3610 | Gift from Wade Winkler laboratory (University of Maryland, College Park, MD) (4) | MA-002 |
| ***Δeps*** | epsH::tet$^{R}$ | Gift from Roberto Kolter laboratory (Harvard Medical School, Cambridge, MA) (5) | MA-013 |
| ***Δphrc*** | phrC::neo$^{R}$ | (6) | MA-109 |
| ***Δopp*** | oppD::cm$^{R}$ | (6) | MA-130 |
| ***ΔtasA*** | sacA::$P_{yqxM}$-trsA216-YFP, cm$^{R}$ | Gift from Gurol Suel laboratory (UC San Diego, La Jolla, CA) | MA-463 |

## SUPPLEMENTARY VIDEOS

**Supplementary video 1**

Expansion of swarming bacteria in presence of a gradient of kanamycin. Wild type *Bacillus subtilis* was inoculated at the center of the plate. Eventually, bacteria at the swarming front halt due to the presence of the kanamycin diffusive disk placed on a side of a 9 cm Petri Dish 24 h prior inoculation. After the front stops, the swarm is still dynamic since multiple waves of swarming bacteria come from the center of the plate.

**Supplementary video 2**

Swarming *Bacillus subtilis* $\Delta$eps deletion strain was inoculated at the center of the plate. Eventually, bacteria at the swarming front halt due to the presence of the kanamycin diffusive disk placed on a side of a 9 cm Petri Dish 24 h before inoculation.

**Supplementary video 3**

Swarming bacteria during the jamming process visualized as darker cells in the field of view observed at 60x magnification. The speed plot shows the average speed ($\mu$m/s) in the field of view and the blue shade represents S.E.M. The vertical line in the graph indicates the frame of the timelapse in which the average speed was calculated. It can be observed that the jam makes the overall speed to drop by half of the initial magnitude.

**Supplementary video 4**

Process of jams and islands formation under 10x magnification. The left panel shows swarming bacteria continuously jamming. The jams look like dark localized small regions in the field of view which continuously appear and disappear. The right panel shows the same scenario 10 min later, when the islands become more stable. Islands look like extended dark regions in the field of view which are highly dynamic and with highly fluctuating boundaries.

**Supplementary video 5**

Coexistence between a second layer of swarming bacteria (darker region in the field of view) and a surrounding monolayer of swarming cells under 40x magnification. The boundaries of the island continuously exchange cells with the monolayer surrounding it. Within the island, cell seem to meander across the layers.

**Supplementary video 6**

Formation of multilayers in a swarming plate with a kanamycin diffusive disk. The multilayer starts forming in the region near the disk where multiple islands appear. The islands become very elongated at the front and they grow in size until they merge. The nucleation and merging of islands were observed up to 4 layers before we lost the ability to recognize further transitions due to a flattening of the image contrast. In the opposite side of the plate, away from kanamycin, the islands appear and merge homogeneously in the whole region.

**Supplementary video 7**

Time-lapse of accumulation of bacteria over time when they are being continuously irradiated by UV light in a region that is as large as the field of view. Eventually, bacteria accumulation gives rise to the formation of localized islands, which appear as dark regions in the field of view, finally leading to a confluent second layer.

**Supplementary video 8**

Process of island formation when the swarming front hits a physical barrier which is placed just on the right of the field of view. Islands start forming in the region closer to the barrier and then propagate towards the opposite direction. After the initial island formation, we can see that the swarm is still dynamic and keep forming multiple layers through island formation and merging.

**Additional references**


1. A. W. Bauer, W. M. M. Kirby, J. C. Sherris, M. Turck, Antibiotic Susceptibility Testing by a Standardized Single Disk Method. *Am. J. Clin. Pathol.* **45**, 493–496 (1966).
2. S. Preibisch, S. Saalfeld, P. Tomancak, Globally optimal stitching of tiled 3D microscopic image acquisitions. *Bioinformatics* (2009) https:/doi.org/10.1093/bioinformatics/btp184.
3. D. B. Adimpong, *et al.*, Antimicrobial susceptibility of bacillus strains isolated from primary starters for african traditional bread production and characterization of the bacitracin operon and bacitracin biosynthesis. *Appl. Environ. Microbiol.* **78**, 7903–7914 (2012).
4. I. Irnov, W. C. Winkler, A regulatory RNA required for antitermination of biofilm and capsular polysaccharide operons in Bacillales. *Mol. Microbiol.* **76**, 559–575 (2010).
5. S. S. Branda, J. E. Gonzalez-Pastor, S. Ben-Yehuda, R. Losick, R. Kolter, Fruiting body formation by Bacillus subtilis. *Proc. Natl. Acad. Sci.* **98**, 11621–11626 (2001).
6. M. Asally, *et al.*, Localized cell death focuses mechanical forces during 3D patterning in a biofilm. *Proc. Natl. Acad. Sci. U. S. A.* **109**, 18891–18896 (2012).